Numerical modeling of the underground mining stope stability considering time-dependent deformations via finite element method

http://dx.doi.org/10.1590/0370-44672023770080

Marinésio Pinheiro de Lima[1,2]
https://orcid.org/0000-0002-7204-8826
Leonardo José do Nascimento Guimarães[1,3]
https://orcid.org/0000-0001-6803-6024
Igor Fernandes Gomes[1,4]
https://orcid.org/0000-0003-2474-383X

[1]Universidade Federal de Pernambuco - UFPE,
Departamento de Engenharia Civil,
Recife – Pernambuco - Brasil.

E-mails: [2]marinesio.pinheiro@ufpe.br,
[3]leonardo.guimaraes@ufpe.br, [4]igor.fernandes@ufpe.br

Abstract

The main objective of this study is to evaluate the hanging wall stability of the mining stopes resulting from the open stope underground mining method, taking into account the exposure time of the wall sans any support, through numerical simulation, using an elasto-viscoplastic model formulated for the finite element method. In order to carry out the simulation, a real application case was chosen: the extraction of a mining block from the underground zinc mine of Nexa Resources, in the municipality of Vazante-MG, which operates through the open stope mining method, where the values of unplanned dilution are known. The stability of the stope's hanging wall was analyzed through two instability indicators, the horizontal displacements and the minor principal stress, simulated in a two-dimensional perpendicular section and in the center of the stope. The results obtained in the simulations were coherent with the real results that occurred in the stope, and with the rheological behavior of the rocks, since the unstable regions increase with the exposure time without any type of support used, which shows that the model used is a good alternative for prediction of the dilution and the evolution of instability areas of the stope wall according to its exposure time.

Keywords: numerical modeling, underground mining, open stopes, elasto-viscoplasticity.

1. Introduction

The open stope mining method is one of the most used in underground mining of metallic minerals. It is characterized by low costs, high recovery, high productivity and good operational safety. Its application is mostly perceived in the extraction of massive or tabular ore bodies whose host rocks are competent, with few restrictions on the shape and size of the openings. Allied to new drilling and blasting technologies, they allow for the opening of large sized stopes, making it the lowest cost underground mining method available. (Dzimunya *et al.*, 2018; Villaescusa, 2014).

The high productivity levels in the opening of the stopes cause a redistribution of stresses that can cause undesirable phenomena, such as natural rock explosions (rockbursts), unplanned dilution and instability of important regions for the mine's production process. The stope projects contemplate the planned dilution, which is the mixture of sterile material with the ore in its mining process, whereas the unplanned dilution is the mixture of the sterile material disassembled outside the planned limits of the stope, and originates in detonations and in displacements that are directly linked to the stability of

the stope walls.

The stope project addresses empirical and numerical methodologies, aiming at promoting a safe environment and minimizing unplanned dilution. One of the most popular empirical methods in mining for scaling enhancements is the Stability Graphic Method, proposed by Mathews (1981) and later revised by several authors. However, the evolution in computer processing capacity has enabled the development and popularization of numerical models which are capable of predicting unplanned dilution in stope designs.

The finite element method (FEM) is a numerical technique widely used to analyze engineering problems. When applied to the design of stope in underground mines, it plays an important role in simulating unplanned dilution. Its use can be exemplified in the articles by Cepuritis *et al.* (2010), Abdellah, Hefni and Ahmed (2020), Cordova, Zingano and Gonçalves (2022) Guggari, Kumar and Budi (2023), who used elastic and elastoplastic models via the finite element method (FEM) to predict unplanned dilution.

The responses of the rock mass to underground excavations can be understood as time-independent and time-dependent mechanical behavior. Elastic and plastic behaviors are distinct and independent of time. The time-dependent mechanical behavior is characterized by slow and continuous deformation under a state of constant stress called creep. Detailed studies on the creep of geomaterials can be found in the studies of Zhao *et al.* (2017), Paraskevopoulou & Diederichs (2018), Borja & Yin (2019).

Perzyna (1966) first proposed the general concept of elasto-viscoplaticity, which defines the variation of viscoplastic deformations over time, as a viscosity-dependent tensor, as well as the maximum resistance provided by the creep function and the potential variation plastic in relation to the stress tensor. Since then, the elasto-viscoplastic behavior of rocks has been discussed, based on field investigations, laboratory tests, constitutive models and numerical analyses.

Numerical models capable of simulating time-dependent behavior have been developed for long-term engineering solutions. Gioda & Cividini (1994) presented simple linear and non-linear constitutive laws capable of describing this phenomenon, using the finite element method. Lazari *et al.* (2019) reassessed Perzyna-type viscoplasticity for constitutive modeling of granular geomaterials, with an emphasis on simulating rate/time effects of different magnitudes. Harahap & Chang-Yu (2020) investigated the time-dependent behavior of a diaphragm wall and ground surface for a typical excavation in soft clay using two-dimensional finite element analysis. Kabwe Karakus & Chanda (2020) presented a viscoelastic viscoplastic constitutive model and implemented the constitutive equations in FLAC3D to simulate deformations responsible for compression inside a tunnel. Xu (2023), proposed a nonlinear rheological model with a non-stationary creep parameter, with FEM formulation, to represent the tertiary creep characteristics in soil slopes.

The main objective of this research is to evaluate the stability of the hanging wall of the stopes from the Open Stope underground mining method, taking into account its exposure time without any type of support. For this, an elasto-viscoplastic model with formulation for FEM was used in order to predict the evolution of instability indicators that contribute significantly to the unplanned dilution of the stope. The simulation was carried out in the finite element code CODE_BRIGTH, using the elasto-viscoplastic model with Mohr Coulomb plastification criteria and the viscous model based on Perzyna's theory, implemented at the Laboratory of Computational Methods in Geomechanics (LMCG) at UFPE.

2. Materials and methods

The research consists of applying an elasto-viscoplastic model for the simulation of the instability caused by the effect of the exposure time of the open stope walls through the open stope mining method, for which the finite element code CODE BRIGTH was used, implemented with the constitutive models of Mohr Coulomb and Perzyna. The two-dimensional model was elaborated in plane deformation of finite elements representing a perpendicular section in the center of the stope, aiming at analyzing the evolution of two instability indicators, the horizontal displacements and the minor principal stress in the hanging wall.

2.1 The model adopted

The model adopted incorporates the elastic, plastic and viscoplastic behavior of the rock mass, through the Mohr-Coulomb plasticization criterion with viscous regularization of plasticity based on the Perzyna model.

The limiting stress state between elastic and plastic behavior is determined by the creep function $F(\sigma, K)$, defined as a function of the stress state (σ) and the plastic parameters of the material (K). This function defines a surface in the stress space, called the creep surface. When the stresses are found inside the surface, we say that $F(\sigma, K) < 0$ and the material behaves elastically. When the stress state reaches the surface, we say that $F(\sigma, K) = 0$, and plastic deformations occur. The region outside the surface is represented by $F(\sigma, K) > 0$ and defines the plastically unacceptable stresses. Viscoplastic behavior is defined as a process of plasticity regularization, where stresses can exceed the creep surface $F(\sigma, K) > 0$, and viscous properties are considered (Gomes, 2009).

The constitutive model adopted and the viscoplastic formulation of the model are then presented.

2.1.1 The Constitutive model adopted

The model uses the Mohr-Coulomb plasticization criterion, which is characterized by the cohesion (c) and the internal friction angle (ϕ). Considering the isotropic material, the Mohr Coulomb creep surface can be defined as a function of the invariants expressed by Equation 1, where p is the effective mean stress, J is the deviating stress, and θ is the Lode angle and $g(\theta)$ is the function of Lode.

$$F(\boldsymbol{\sigma}, k) = J - \left(\frac{c}{\tan\phi} + p\right) g(\theta) = 0 \quad (1)$$

Where $g(\theta)$ is the function of Lode, defined by Equation 2.

$$g(\theta) = \frac{sen\ \phi}{cos\ \theta + \frac{sen\ \theta sen\ \phi}{\sqrt{3}}} \quad (2)$$

The adopted model shows the $F(\sigma, K)$ function defining both the plastification criterion and the direction of plastic deformations, considering a bilinear law of softening, for which the shear resistance properties of the material (in this case, cohesion and effective friction angle) are reduced due to the occurrence of deviating plastic deformations. According to Potts & Zdravkovic (1999), in the Mohr-Coulomb model, the resistance parameters vary linearly with the accumulated deviating plastic deformations.

2.1.2 Viscoplastic formulation

The elasto-viscoplastic model adopted is that of Perzyna, which is implemented in the finite element code CODE_BRIGHT. Its structure is based on the mathematical formulation of the plasticity theory, with viscous effects only in the plastic regime where the creep surface changes to new stress states, according to time. Total deformation is decomposed into two parts, elastic and viscoplastic, as seen in Equation 3.

$$\dot{\boldsymbol{\varepsilon}} = \dot{\boldsymbol{\varepsilon}}^{e} + \dot{\boldsymbol{\varepsilon}}^{vp} \quad (3)$$

Stress increment is defined by the elastic constitutive tensor and by the total deformation rate, as seen in Equation 4.

$$\dot{\boldsymbol{\sigma}} = \mathbf{D}_{e} (\dot{\boldsymbol{\varepsilon}} - \dot{\boldsymbol{\varepsilon}}^{vp}) \quad (4)$$

The viscoplastic deformation rate is obtained as seen in Equation 5.

$$\dot{\boldsymbol{\varepsilon}}^{vp} = \dot{\Lambda} \cdot \mathbf{m} \quad (5)$$

Where $\dot{\Lambda}$ is the viscoplastic multiplier and $\mathbf{m}$ is the second-order tensor that determines the direction of the viscoplastic strain rate, which in the case of associated plasticity adopted here, is derived from the creep function, according to Equation 6.

$$\mathbf{m} = \frac{\partial F(\boldsymbol{\sigma}, k)}{\partial \boldsymbol{\sigma}} \quad (6)$$

Viscoplastic multiplier Λ is defined by a monotonic function and a viscous parameter η, as seen in Equation 7.

$$\Lambda = \frac{\langle \phi(F(\boldsymbol{\sigma}, k)) \rangle}{\eta} \quad (7)$$

Considering the associated viscoplasticity, the viscoplastic strain rate and the internal variable k are formulated as a function of an elastic tensor $\boldsymbol{D}$, by a monotonic function, which is defined by Equation 8.

$$\dot{\boldsymbol{\varepsilon}}^{vp} = \frac{\langle \phi(F(\boldsymbol{\sigma}, k)) \rangle}{\eta} \frac{\partial F(\boldsymbol{\sigma}, q)}{\partial \boldsymbol{\sigma}} \quad (8)$$

For implementation in finite elements, the Perzyna model considers the adoption of a tangent matrix $\mathbf{D^{**}}$ as a function of the viscoplastic strain gradient applied to the global stiffness matrix of the discretized stress equilibrium equation. From the relationship between the elastic tensor $\mathbf{D}$ and a viscoplastic tensor $\mathbf{D^{*}}$ defined in Equation 9. The viscoplastic tensor $\mathbf{D^{*}}$ has the form of Equation 10, and it is obtained as a function of a strain velocity gradient, which according to the Theory of Perzyna, the strain velocity gradient matrix is defined by Equation 11 (Zienkiewicz & Taylor, 1999).

$$\mathbf{D^{**}} = \mathbf{D^{*}}\ \mathbf{D} \quad (9)$$

$$\mathbf{D^{*}} = \left[\mathbf{I} + \mathbf{D} \frac{\partial \varepsilon^{vp}}{\partial \sigma}\right]^{-1} \quad (10)$$

$$\frac{\partial \varepsilon^{vp}}{\partial \boldsymbol{\sigma}} = \frac{\partial}{\partial \boldsymbol{\sigma}} \left[\frac{\Delta t \langle \varphi(F) \rangle}{\eta} \cdot \frac{\partial F}{\partial \boldsymbol{\sigma}}\right] \quad (11)$$

Where Δt is the time interval; η is the viscous material parameter during viscoplastic deformation; F fluence function, and σ the stress tensor.

2.2 Application case

In order to carry out the simulation by applying the described elasto-viscoplastic model, a real case of the Nexa Resources Zinc Underground Mine, located in the municipality of Vazante (northwest of Minas Gerais state) was chosen, and it was presented in detail by Charbel (2015).

The mining method used in the mine is the open-stope type, having stopes filled with sterile rock sans cement. For the elaboration of the model, mining block 9140 was chosen at level 420 of the Vazante mine. Figure 1(a) illustrates the geometric characteristics of mining block 9140 - its base is 268.5 meters from the surface. A simulation of a two-dimensional section was carried out in the center of the stope and its characteristics are shown in Figure 1(b), containing the dimensions of the stope excavated in the willemite breccia that is embedded in dolomitic breccias and dolomites.

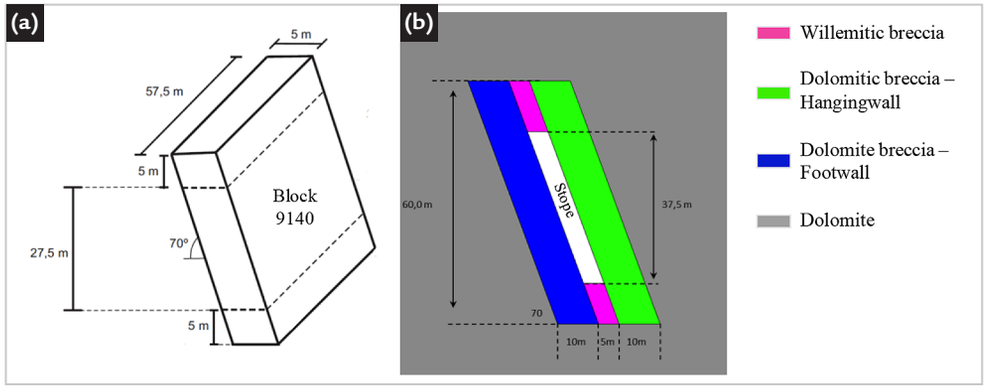

Figure 1 – (a) Mining block geometry (Modified from Charbel, 2015); (b) Geometry of the two-dimensional section in the NW-SE direction indicating the positioning of the stope and the lithologies involved.

The in situ stress state is described in Table 1:

Table 1 - In situ stress state in the NW-Se direction.

γ (MN/m^3)	h (m)	K^{NW-SE}	σ_v (MPa)	σ_h (Mpa)
0.027	268.5	1.0	7.95	7.95

Source: Charbel (2015).

In the Vazante mine, the unplanned dilution process is linked to the displacements that occurred in the hanging wall of the stopes. Thus, the analysis was carried out on the hanging wall of the stope, whose characteristics are described in Table 2.

Table 2 - Block 9140 hanging wall features raised in the mine.

Hanging wall length	Hanging wall width	Hanging wall area	Stope volume	Hanging wall ELOS	Stope dilution
57.5 m	39.9 m	2294.25 m^2	11471.25 m^3	3.82 m	43.3%

Based on Clark's Equivalent Linear Overbreak/Slough (ELOS) theory (1998) expressed by Equation 12, and the quantification of unplanned dilution expressed by Equation 13, according to Pakalnis (1986), Equation 14 is obtained, and it expresses the unplanned dilution as a function of ELOS. The graph in Figure 2 shows the behavior of unplanned dilution for an increase in ELOS up to 15 m, which is a sufficient value to analyze the simulation results.

$$Elos = \frac{Overbreak\ Volume\ (m^3)}{Face\ Area\ (m^2)} \quad (12)$$

$$Dilution_{NP} = \frac{Overbreak\ Volume}{Overbreak\ Volume + Stope\ Volume} \times 100\% \quad (13)$$

$$Dilution_{NP} = \frac{(ELOS \times Face\ Area)}{(ELOS \times Face\ Area) + Stope\ Volume} \times 100\% \quad (14)$$

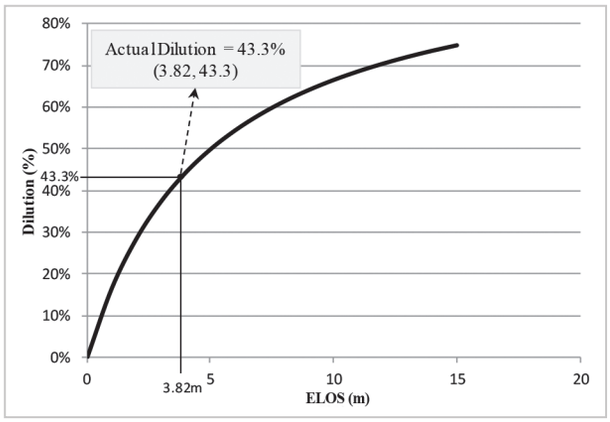

Figure 2 - Characteristic graph of dilution as a function of ELOS for the hanging wall of block 9140, showing the actual dilution that occurred in the stope.

2.2.1 Finite elements model

The model represents a two-dimensional perpendicular section in the center of mining block 9140 of the Vazante mine, at level 420. The simulation section has a domain of 540 m x 540 m. An unstructured finite element mesh was used, with 22626 triangular-like elements and 11342 nodes whose characteristics, boundary conditions and mesh detail in the area close to the excavation are shown in Figure 3.

The geomechanical parameters of the lithologies were determined by the team at the Vazante mine; the Hoek-Brown (2002) criterion was used to determine the rock mass characteristics by lithology, which is treated here as a continuous and isotropic equivalent massif (Table 3).

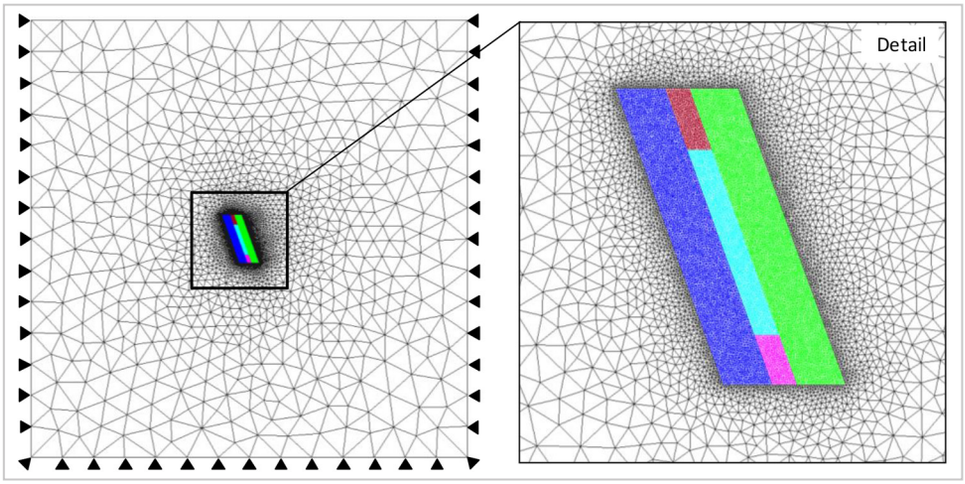

Figure 3 - Finite element mesh with detailing the stope.

Table 3 - Hoek-Brown parameters for each lithology.

Hoek-Brown Parameters	Dolomite	Hanging wall Pink Dolomitic Breccia	Footwall Gray Dolomitic Breccia	Willemitic Breccia
σ_{ci} (MPa)	124	136	101	108
GSI	60	42	42	44
m_i	12.5	23.9	23.9	20.9
Ei (GPa)	58	42	55	63
m_b	2.99564	3.01153	3.01153	2.82851
s	0.011744	0.00158933	0.00158933	0.001985
a	0.502841	0.509923	0.509923	0.508658

Information: σ_{ci} = Resistance to the uniaxial compression of the rock matrix; E_i = Modulus of rock matrix elasticity; m_i, m_b, s and a = Hoek-Brown parameters for the rock matrix.

The cohesion c and the friction angle ϕ are obtained through an adjustment of the average linear relationship to the Hoek-Brown and Mohr-Coulomb envelope, through use of the RocLab 1.0 software from Rocscience. The residual cohesion values were considered equal to zero, in view of modeling the rupture, and the residual friction angle was considered equal to one, for numerical convenience. Table 4 shows the model input parameters for each lithology.

Table 4 - Model Input Parameters.

Characteristics	Dolomite	Hanging wall Pink Dolomitic Breccia	Footwall Gray Dolomitic Breccia	Willemitic Breccia
Density (MN/m^3)	0.027	0.030	0.027	0.035
c_i (MPa)	2.40	1.90	1.75	1.98
c_r (MPa)	2.40	0	0	0
ϕ_i (°)	51.7	52.1	50.0	48.8
ϕ_r (°)	51.7	1	1	1
E_{mr} (GPa)	30	12	10	13
Poisson's ratio	0.20	0.20	0.20	0.20
Perzyna viscous parameter	1.0 x 10^6	1.0 x 10^6	1.0 x 10^6	1.0 x 10^6

Information: c_i = Initial Cohesion; c_r = Residual Cohesion; ϕ_i = initial internal friction angle; ϕ_r = residual internal friction angle; E_{mr} = Modulus of rock matrix elasticity.

The simulation was carried out using the CODE BRIGHT finite element code within the total time of 6000 seconds. In the interval from 0 to 4000 seconds, the initial stresses were obtained through the geostatic stress state. At time T_1 = 4000 seconds, the stope was opened, remaining open until time T_2 = 6000 seconds. Two simulations were carried out; in the first, the viscous parameter value of 1.0 x 10^6 was adopted, large enough for the model to behave in an elastoplastic manner. In the second simulation, the value of the viscous parameter was reduced by half, so that viscoplastic deformations occur, in order to analyze the instability indicators in the range from T_1 to T_2 for the two behaviors. The viscous parameter varies from 0 to +infinity, Its relationship with the time step defines the magnitude of the flow rule penalty, so that when it tends to zero, it can lead to convergence problems for material failure. Therefore, the value of 0.5 x 10^6 was defined experimentally, aiming to obtain the lowest value of the viscous parameter with convergence of the problem.

3. Results and discussion

The evaluation of the evolution of two instability parameters, the horizontal displacements and the minor principal stress that occurred in the center of the hanging wall of the enhancement took place, indicating the ELOS value at the instant of opening of the stope (T_1=4000s) and at the end of the simulation (T_2=6000s).

3.1 Horizontal displacements for the viscous parameter of 1.0 x 10^6

According to Charbel (2015), isovalue curves of displacements greater than or equal to 1cm coincided satisfactorily with the displacements measured on the hanging wall of the mine stopes. Thus, the ELOS referring to 1cm horizontal displacements was measured. The evaluation of the horizontal displacements was carried out along the horizontal line in the center of the hanging wall up to a distance of 20 meters, as illustrated in Figure 4(a), which shows the = 1 cm horizontal displacements simulated at times T_1=4000s and T_2= 6000s.

In Figure 4(b), it is observed that the amplitude of the displacements equal to 1cm at the moment of the stope opening (T_1) reaches the value of 3.3 m, which will be equivalent to the ELOS for that moment. As for the values at instant T_2, displacements equal to 1 cm reach a distance of 5.04 m, increasing the ELOS value from 3.3 m to 5.04 m in an interval of 2,000s.

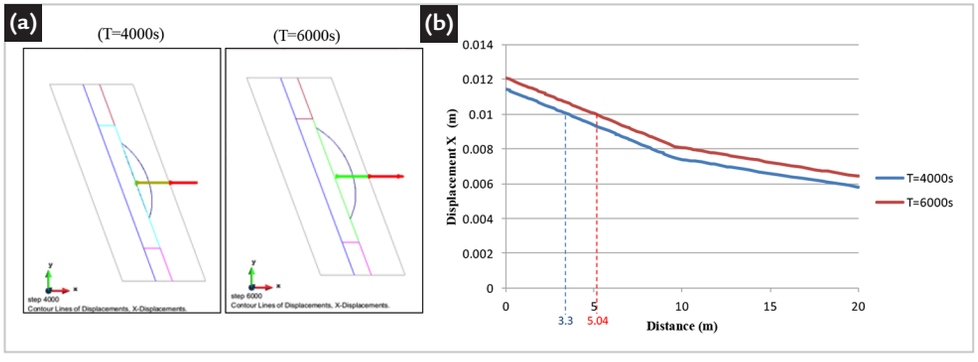

Figure 4 - (a) Isovalue line of = 1cm horizontal displacements in T_1 e T_2 instants; (b) Horizontal displacement values in the center of the hanging wall at instants T_1 e T_2.

Figure 5 shows the characteristic dilution graph of the hanging wall, where the simulated dilution values can be compared with the real values perceived in the stope. It can be seen that, at T_1, the simulated dilution was 39.8%. At instant T_2, an increase in dilution to 50% is observed.

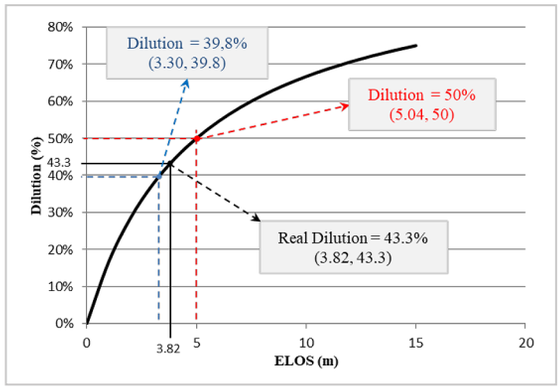

Figure 5 - Comparison between simulated dilution values and real dilution value in instants T_1 e T_2 for the viscous parameter of 1.0 x 10^6.

3.2 Low confinement region for the viscous parameter of 1.0 x 10^6

Minor Principal Stress is the second parameter used to define the ELOS of the stope Face. The evaluation consists of defining the amplitude of the low confinement region ($\sigma_3 \leq 0$) along the horizontal line in the center of the hanging wall of the stope. Figure 6(a) shows the result of the simulation containing the isovalue curves of $\sigma_3 \leq 0$ at times T_1=4000s and T_2=6000s. The graph in Figure 6(b) shows the values of σ_3 along the horizontal line in the center of the hanging wall at instants T_1 and T_2, defining the ELOS of 4.31 meters for T_1 and 6.32 meters for T_2.

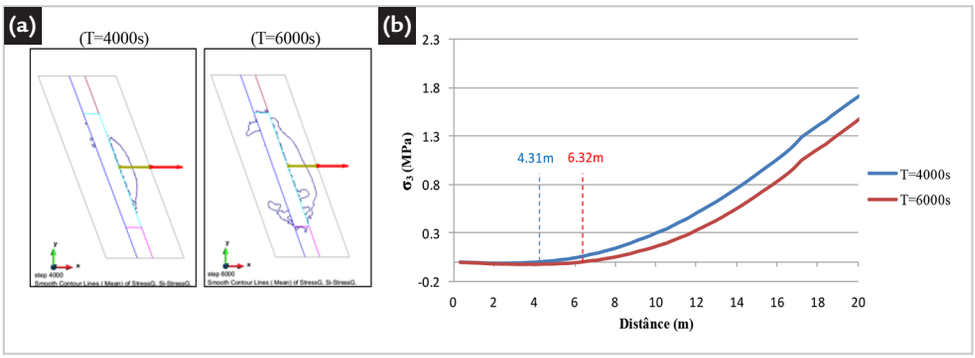

Figura 6 - (a) Low confinement regions ($\sigma_3 \leq 0$) at instants T_1 and T_2; (b) σ_3 values along the line in the center of the hanging wall at instants T_1 e T_2 for the viscous parameter of 1.0 x 10^6.

In Figure 7, the real dilution values can be compared to the simulated dilution through the behavior of the low confinement regions ($\sigma_3 \leq 0$). At instant T_1, a simulated dilution of 44.4% is observed, and at T_2, the dilution reaches a value of 55.8%.

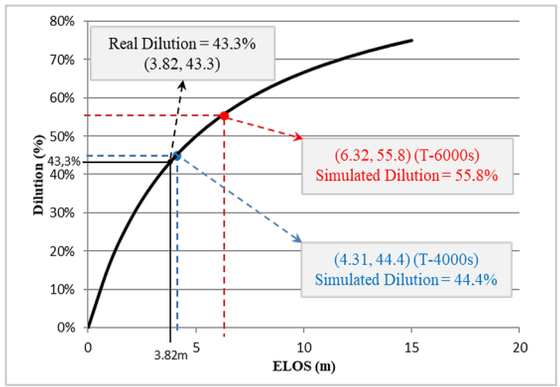

Figure 7 - Comparison between simulated values and the real value of dilution at instants T_1 e T_2 through the simulation of low confinement areas ($\sigma_3 \leq 0$) for the viscous parameter of 1.0 x 10^6.

According to the results, it appears that the determination of the ELOS through the modeling of the low confinement regions proved to be a little more accurate, which led us to carry out the analysis of the Perzyna viscous parameter through this indicator.

3.3 Low confinement region for the viscous parameter of 0.5 x 10^6

The viscous parameter was reduced from 10^6 to 5 x 10^5, where a more accurate result was obtained for unplanned enhancement dilution at instant T_1, shown in Figures 8(a) and 8(b).

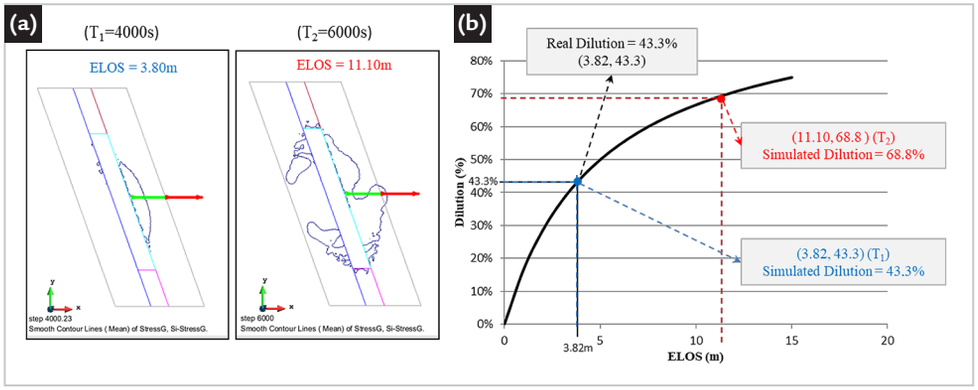

Figure 8 - (a) ELOS at instants T_1 and T_2 with viscous parameter of 5 x 10^5; (b) Dilution values at instants T_1 and T_2 with viscous parameter of 5 x 10^5.

With the reduction of the viscous parameter to 5 x 10^5, a significant increase in the deconfinement region can be seen, from the interval between T_1 and T_2, with the simulated dilution at the moment of opening the enhancement (T_1) being equal to the real value of the dilution that occurred in the 43.3% enhancement. At time T_2, the ELOS has a significant increase, from 3.43m to 11.10m, which represents an increase of 25.4% in the simulated dilution. This occurs due to the decrease in the viscous parameter, which provides an increase in the viscoplastic deformation rate described by Equation 8, meaning an increase in viscoplastic deformations in the interval between T_1 and T_2, while the simulation with the higher viscous parameter means less viscoplastic deformations, having the model behave like an elastoplastic model. This shows that the model can be easily manipulated to predict deformations depending on the simulation time, and adapt the results to real intervals. This article did not address the adaptation of simulation times to real intervals.

4. Conclusions

According to the results obtained in the numerical simulations via the finite element method, it was observed that both the displacements and the low confinement regions are good indicators for predicting the unplanned dilution of the rock mass in question. The elasto-viscoplastic model used proved to be coherent with the theories of the rheological behavior of rocks, and presented good ability to adapt the parameters to predict displacements that occurred in the hanging wall of the stope. The behavior of the indicators over the exposure time in the performed simulations showed viscoplastic deformations, and the longer the exposure time, the greater the ranges of those indicators, and consequently, the greater the unplanned dilution. The value of the viscous parameter imposes different behaviors on the rock mass rheology, whereupon the lower the value of the parameter, the faster the evolution of the indicators occurs, causing a greater amplitude at the end of the simulation. Thus, observed is a good applicability of the model for predicting dilution in open stope by the open stope underground mining method, as well as providing a stress-strain analysis over time in pillars and galleries that are in the areas of influence within the excavations.

References

ABDELLAH, W. R. E.; HEFNI, M. A.; AHMED, H. M. Factors influencing stope hanging wall stability and ore dilution in narrow-vein deposits: part 1. ***Geotechnical and Geological Engineering***, v. 38, p. 1451-1470, 2020.

BORJA, R. I.; YIN, Q.; ZHAO, Y. Cam-Clay plasticity. Parte 9: on the anisotropy, heterogeneity, creep of shale. ***Computer Methods in Applied Mechanics and Engineering***, v. 360, p. 1-25, 2019. Available in: https://doi.org/10.1016/j.cma.2019.112695

CEPURITIS, P. M.; VILLAESCUSA, E.; BECK, D. A.; VARDEN, R. Back analysis of over-break in a longhole open stope operating using non-linear elasto-plastic numerical modelling. *In*: SYMPOSIUM OF ROCK MECHANICS AND FIFTH CANADA-US ROCK MECHANICS SYMPOSIUM, 44., 2010. ***Proceedings*** **[...]**. 2010, Salt Lake City. p. 27-30 June, 2010. Available in: http://dx.doi.org/10.13140/2.1.4932.8641

CHARBEL, P. A. ***Gerenciamento de risco aplicado à diluição de minério.*** 2015. 406 f. Tese (Doutorado em Engenharia Civil e Ambiental) - Departamento de Engenharia Civil e Ambiental, Universidade de Brasília, Brasília, DF, 2015.

CLARK, L. M. ***Minimizing dilution in open stope mining with a focus on stope design and narrow vein longhole blasting.*** 1998. 336 f. MASc thesis, University of British Columbia, Department of Mining and Mineral Processing Engineering, 1998.

CORDOVA, D. P.; ZINGANO, A. C.; GONÇALVES, Í. G. Unplanned dilution back analysis in an underground mine using numerical models. ***REM - International Engineering Journal,*** v. 75, p. 379-388, 2022.

DZIMUNYA, N.; RADHE, K.; WILLIAM, C. M. Design and dimensioning of sublevel stoping for extraction of thin ore (< 12 m) at very deep level: a case study of konkola copper mines (kcm), Zambia. ***Mathematical Modelling of Engineering Problems,*** v. 5, p. 27-32, 2018. Available in: https://doi.org/10.18280/mmep.050104

GIODA, G.; CIVIDINI, A. Finite element analysis of time dependent effects in tunnels. *In*: ***Visco-Plastic behaviour of geomaterials.*** Vienna: Springer Vienna, 1994. p. 209-243.

GOMES, I. F. ***Implementação de métodos explícitos de integração com controle de erro para modelos elastoplásticos e visco-elastoplásticos.*** 2009. 188 f. Tese (Doutorado em Engenharia Civil) - Programa de Pós Graduação em Engenharia Civil - Universidade Federal de Pernambuco, Recife, PE, 2009. 188 f.

GUGGARI, V. B.; KUMAR, H.; BUDI, G. Numerical analysis for assessing the effects of crown pillar thickness on ore dilution around the sub-level open stops. ***Ain Shams Engineering Journal,*** p. 102301, 2023.

HARAHAP, S. E.; Chang-Yu, Ou. Finite element analysis of time-dependent behavior in deep excavations. ***Computers and Geotechnics,*** v. 119, p. 103300, 2020.

HOEK, E.; CARRANZA, T. C.; CORKUM, B. Hoek-Brown failure criterion. mining and tunnelling innovation and opportunity. *In*: NORTH AMERICAN ROCK MECHANICS SYMPOSIUM, *5*; TUNNELLING ASSOCIATION ASSOCIATION OF CANADA CONFERENCE, 17, 2002, Toronto, ***Proceedings*** **[...]** p. 267-273, 2002.

KABWE, E.; KARAKUS, M.; CHANDA, E. K. Creep constitutive model considering the overstress theory with an associative viscoplastic flow rule. ***Computers and Geotechnics,*** v. 124, 2020.

LAZARI, M.; SANAVIA, L.; PRISCO, C.; PISANÒ, F. Predictive potential of Perzyna viscoplastic modelling for granular geomaterials. ***International Journal for Numerical and Analytical Methods in Geomechanics,*** v. 43, n. 2, p. 544-567, 2019.

MATHEWS, K. E.; HOEK, E.; WYLIE, D. C.; STEWART, S. B. V. ***Prediction of stable excavation spans for mining at depths below 1,000 m in hard rock mines.*** Ottawa: CANMET, 1981. (Canmet Report DSS Serial No. OSQ80-00081).

PAKALNIS, R. T. ***Empirical stope design at the ruttan mine, Sherritt Gordon MinesLtd.*** PhD. thesis - University of British Columbia, Department of Mining and Mineral Processing Engineering, 1986. 276 f.

PARASKEVOPOULOU, C.; DIEDERICHS, M. Analysis of time-dependent deformation in tunnels using the Convergence Confinement Method, ***Tunnelling and Underground Space Technology,*** v. 71, p. 62-80, 2018. Available in: https://doi.org/10.1016/j.tust.2017.07.001

PERZYNA, P. Fundamental problems in viscoplasticity. In: CHENYI, G. G. ***Advances in applied mechanics,*** 9. ed. New York and London: Academic Press, 1966. p. 243-377.

POTTS, M. D.; ZDRAVKOVIĆ, L. L. ***Finite element analysis in geotechnical engineering.*** London: Thomas Telford Publishing, 1999.

VILLESCUSA, E. ***Geotechnical design for sublevel open stoping.*** London, New York: Boca Raton. CRC Press, 2014.

XU, J. Failure process of saturated granite residual soil slope: a 3D viscoelastic-plastic finite element modeling approach with nonstationary parameter creep. ***Bull Eng Geol Environ,*** v. 82, n. 276, 2023. Available in: https://doi.org/10.1007/s10064-023-03298-x

ZHAO, Y, WANG, Y. WANG, W, WAN, W. TANG, J. Modeling of non-linear rheological behavior of hard rock using triaxial rheological experiment. ***International Journal of Rock Mechanics & Mining Sciences,*** v. 96 p. 66-75, 2017. https://doi.org/10.1016/j.ijrmms.2017.01.004

ZIENKIEWICZ, O. C.; TAYLOR, R. I. ***The finite element method.*** London: Mc-Graw-Hill Book Company, 1999. v. 2.

Received: 14 July 2023 - Accepted: 14 December 2023.